An Uncertainty-driven Analysis for Delayed Mapping SLAM

Davide Dorigoni, Daniele Fontanelli
University of Trento - Dep. of Industrial Engineering
Trento, Italy
Email: daniele.fontanelli@unitn.it

***Abstract*—This papers deals with the analysis of the delayed SLAM problem from the perspective of the uncertainties involved in the process. We consider an autonomous mobile robot moving in an environment and equipped with noisy encoders, used for the ego-motion reconstruction, and with a LIDAR for indoor features detection. We adopt an Extended Kalman Filter (EKF) based solution and we analyse the effect of the length of the delayed measurement window on the system uncertainties. The analysis covers the standard LIDAR measurements, but it is also extended to range-only measurements. Mont Carlo simulation results are provided on synthetic indoor environments for both the cases.**

***Index Terms*—Delayed Mapping, Extended Kalman Filter, SLAM problem**

I. Introduction

Autonomous systems applied to natural environments as well as industrial robots have the necessity to localise themselves in the operational space using on-board or environmental sensing systems. To improve the autonomous capabilities of such systems, no-knowledge is given upfront about the environmental structure, which asks for Simultaneous Localisation and Mapping (SLAM) solutions [1], [2]. A solution to a SLAM problem allows a mobile agent to estimate both the sensed environmental features (thus generating a *map*) and the location of the system (i.e., the *localisation* problem) with respect to the reconstructed map contextually. Of course, this is a chicken and egg problem that is prone to unbounded uncertainties if additional constraints are not satisfied, i.e. loop closure event [1].

A taxonomy of the different SLAM solutions can be given in terms of the different sensors adopted. Probably the most popular solutions rely on visual sensors [3], [4], either monocular cameras, stereo cameras, RGB-D cameras or combinations thereof (e.g., ORB-SLAMv2 [5]). Besides the vision based approaches, one of the most adopted solutions relies on LIDAR sensors, which are adopted for both 2D solutions, such as the FastSLAM [6], or for three dimensional cases, as in IMLS-SLAM [7].

In an effective solution to the SLAM problem, measurement uncertainties play a fundamental role. In this respect, researchers have focused on faulty or wrongly calibrated odometers considering the mapping phase as an ad-hoc optimisation problem, thus generating the so-called Interactive SLAM [8], or proposing map representations that can correctly express the uncertainty content and reduce localisation drifts [9], or by explicitly solving the kidnapped robot problem in the SLAM context using magnetic and radio measurements [10]. Moreover, [11] discussed several ROS-based solutions for visual SLAM and compare them in term of computation time, efficiency and accuracy. Instead, [12] builds their graph-based SLAM solution for drilling machines and considering persistency in the system trajectories measured by a magnetometer.

From a metrological perspective, the problem of relevance is the characterisation of the uncertainties related to both the processes involved (i.e. localisation and mapping) and how they are combined in the final estimation problem (for example, it is actually possible to determine the influence quantities that affects the estimation problem at hand [13]). In this case, the specific estimation algorithm adopted plays a major role. Even though recently deep learning algorithms are becoming more and more popular, especially for visual-based solutions [14], standard Bayesian solutions, such as the Extended Kalman Filters, are still playing the lion's share [15]. The selection of the measurements to inject into the filter in order to increase the overall performance is an investigated problem. For example, [12] uses a two stage uncertainty reduction of the mapped features by travelling two times along the same trajectory, while [8] reformulate the mapping step as an optimisation problem using multiple measurements of the same quantities. This idea is well formalised in delayed SLAM [2] where the features to be mapped are first filtered in isolation and then added to the mapping process. The analysis and characterisation of this process of general applicability is the focus of this paper. In particular, we propose an analysis of the delayed SLAM using LIDARs in terms of the number of measurements needed before the injection of the features in the mapping process. Moreover, we propose a very simple approach that requires less computational burden and does not involve any optimisation algorithm, as instead happens with the widely known bundle adjustment [16]. Finally, we analyse the range-only SLAM as a subset case of the LIDAR measurements.

II. Background Material and Adopted Models

The SLAM problem as considered in this paper is basically an estimation problem using an Extended Kalman Filter (EKF) where the quantities of interest are the vehicle pose

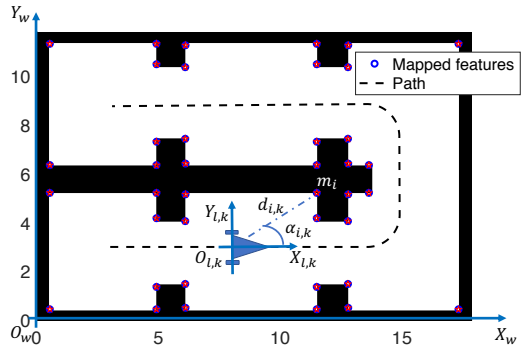

Fig. 1. Vehicle trajectory, measurement example and mapped feature positions.

and the feature positions. The moving platform is assumed endowed with encoders on the rear wheels providing dead reckoning-like information, while it make use of a LIDAR to map static objects inside an indoor environment (i.e., basically walls). Each sensor is supposed to be affected by uncertainties generated by white stochastic processes with known characteristics. Even though the presented approach can be applied to a generic platform moving indoor on an horizontal plane using both ego-motion data and LIDAR measurements, for the sake of the uncertainties derivation we make explicit reference to a unicycle-like vehicle, a typical system that can be found in many industrial and service robotics applications.

A. Platform Model

The kinematic model of a unicycle-like robot is described by the following first-order discrete-time equivalent equations

$$\begin{bmatrix} x_{k+1} \\ y_{k+1} \\ \theta_{k+1} \end{bmatrix} = \begin{bmatrix} x_k \\ y_k \\ \theta_k \end{bmatrix} + \begin{bmatrix} \cos(\theta_k) \\ \sin(\theta_k) \\ 0 \end{bmatrix} v(t)T_s + \begin{bmatrix} 0 \\ 0 \\ 1 \end{bmatrix} \omega(t)T_s, \quad (1)$$

where T_s is the sampling time considered, (x_k, y_k) are the Cartesian planar coordinates of the mid-point of the rear wheels axle at time kT_s and expressed in the reference frame $\langle W \rangle = \{O_w, X_w, Y_w, Z_w\}$ (see Figure 1), and θ_k is the angle between the longitudinal axis of the robot and axis X_w. Moreover, we assume, as customary for controlled robots, that the linear velocity $v(t)$ is constant in the sampling period T_s, i.e. $v(t) = v_k = \text{const}$ for $kT_s \leq t < (k+1)T_s$. The same assumption holds for the angular velocity, i.e. $\omega(t) = \omega_k = \text{const}$. Thus, for SLAM purposes, the robot state can be defined as $s_k = [x_k, y_k, \theta_k]^T$, and hence (1) can be defined as

$$s_{k+1} = s_k + g_v(s_k)v_k + g_\omega(s_k)\omega_k = s_k + g(s_k)u_k, \quad (2)$$

where $u_k = [v_k, \omega_k]^T$ are just the inputs to the system.

B. Measurement Models

The robot is equipped with two measurement devices, i.e., two incremental encoders installed on the rear wheels and a LIDAR for environmental features detection. To characterise the former, the angular velocities $\omega_r(t)$ and $\omega_l(t)$ of the right and left rear wheels can be expressed as a function of the robot input velocities $v(t)$ and $\omega(t)$, i.e.

$$\omega_r(t) = \frac{v(t)}{r} + \frac{l\omega(t)}{2r} \text{ and } \omega_l(t) = \frac{v(t)}{r} - \frac{l\omega(t)}{2r}, \quad (3)$$

where r is the wheels radius and l is the rear inter-axle length. If $\Delta_k = [\omega_r(t)T_s, \omega_l(t)T_s]^T$ denote the angular displacements of the right and left wheels for $kT_s \leq t < (k+1)T_s$ and measured by the encoders in a sampling period T_s, we immediately have by inverting (3) and considering the presence of the reading uncertainties $\varepsilon_k = [\varepsilon_{r,k}, \varepsilon_{l,k}]$ the following encoder model

$$\begin{bmatrix} \overline{v_k}T_s \\ \overline{\omega_k}T_s \end{bmatrix} = \begin{bmatrix} \frac{r}{2} & \frac{r}{2} \\ \frac{r}{l} & -\frac{r}{l} \end{bmatrix} (\Delta_k + \varepsilon_k) = E(\Delta_k + \varepsilon_k). \quad (4)$$

where we use the over-line symbols to denote measurement results. The stochastic sequence ε_k is supposed to be white, stationary and distributed according to $\mathcal{N}(0, \Xi)$, where $E = \text{diag}(\sigma_r^2, \sigma_l^2)$. Hence, the uncertainties on the forward and angular velocities in u_k can be derived from (4), i.e. the uncertainty affecting the inputs u_k is distributed according to $\mathcal{N}(0, Q)$, where $Q = E\Xi E^T$.

As customary, the LIDAR detects a set of points $p_i \in \mathbb{R}^2$ in the plane and expressed in the reference frame of the robot $\langle L_k \rangle = \{O_{l,k}, X_{l,k}, Y_{l,k}, Z_{l,k}\}$, whose origin $O_{l,k}$ is assumed placed in the mid-point of the wheel axle of the vehicle, thus having coordinates $O_{l,k} = [x_k, y_k]^T$ in $\langle W \rangle$ at time kT_s, as depicted in Figure 1 (i.e., the origin $O_{l,k}$ trivially undergoes the same motion of the vehicle). Due to the specific sensing system adopted, all the measured quantities p_i are expressed in polar coordinates, i.e. with a distance and an angle in $\langle L_k \rangle$. Since we are assuming to measure static objects in an indoor environment, e.g. walls, from these collection of points we can derive segments using a Hough transform solution [17] and from the intersections of those segments we can identify corners in the environment, which are regarded as the features to be mapped. The mapped corners are generically denoted with $m_i = [x_i, y_i]^T$, $i \in \mathbb{N}$, and expressed in the frame $\langle W \rangle$, hence the map containing j features is defined as the vector $\mathcal{M}_{j,k} = [m_{1,k}^T, \ldots, m_{j,k}^T]^T$. Each feature is related to the robot state s_k by the following polar coordinates representation in $\langle L_k \rangle$

$$\begin{cases} \overline{d}_{i,k} = \sqrt{(x_k - x_i)^2 + (y_k - y_i)^2} + \tilde{d}_{i,k} \\ \overline{\alpha}_{i,k} = \theta_k - \arctan \dfrac{y_i - y_k}{x_i - x_k} + \tilde{\alpha}_{i,k} \end{cases} \Rightarrow$$
$$z_{i,k} = \begin{bmatrix} \overline{d}_{i,k} \\ \overline{\alpha}_{i,k} \end{bmatrix} = \begin{bmatrix} d_{i,k} \\ \alpha_{i,k} \end{bmatrix} + \begin{bmatrix} \tilde{d}_{i,k} \\ \tilde{\alpha}_{i,k} \end{bmatrix} = h(s_k, m_i) + \rho_{i,k}, \quad (5)$$

where the uncertainties $\rho_{i,k} = [\tilde{d}_{i,k}, \tilde{\alpha}_{i,k}]^T$ are generated by a white, stationary stochastic process and $\rho_{i,k} \sim \mathcal{N}(0, R)$ with $R = \text{diag}(\sigma_d^2, \sigma_\alpha^2)$, which is considered to be not dependent on the particular corner detected, as typical for LIDAR sensors. Moreover, due to the corner detection algorithm considered,

we assume that the uncertainties $\rho_{i,k}$ are equivalent to the LIDAR acquisition noise.

C. Delayed Mapping

This section describes the Bayesian estimator, i.e. an Extended Kalman Filter (EKF), adopted for the application of the delayed SLAM. The standard EKF relies on the models introduced so far and can be synthesised in the following *Prediction* and *Update* steps:

- *Prediction*: denoting with $\hat{p}_k = [\hat{s}_k^T, \hat{\mathcal{M}}_{j,k}^T]^T$ the estimation vector comprising the vehicle state and the mapped entities (we adopt the $\hat{\cdot}$ notation to identify estimated quantities), we have:

$$\begin{aligned} \hat{p}_{k+1}^- &= \hat{p}_k + G(\hat{p}_k)u_k, \\ P_{k+1}^- &= A_k P_k A_k^T + G(\hat{p}_k)\, Q\, G(\hat{p}_k)^T, \end{aligned} \tag{6}$$

  where the matrix $G(\hat{p}_k) = [g(s_k)^T, 0, \dots, 0]^T$ is based on (2) and on the fact that the corner features are static in $\langle W \rangle$ and $A_k = \left(I + \frac{\partial G(\hat{p}_k)u_k}{\partial \hat{p}_k}\right)$;
- *Update*:

$$\begin{aligned} K_{k+1} &= P_{k+1}^- H_{k+1}^T \left(H_{k+1} P_{k+1}^- H_{k+1}^T + R\right)^{-1}, \\ \hat{p}_{k+1} &= \hat{p}_{k+1}^- + K_{k+1}(z_{k+1} - h(\hat{p}_{k+1}^-)), \\ P_{k+1} &= (I - K_{k+1}H_{k+1})\, P_{k+1}^-, \end{aligned} \tag{7}$$

  where K_{k+1} is the Kalman gain, $z_{k+1} = [z_{1,k}^T, \dots, z_{l,k}^T]^T$ is the vector collecting the $2l$ measurements about the j mapped features (notice that not all the mapped corners could be measured at time kT_s, hence $l \leq j$ and that each $z_{i,k}$ comprises two measurement quantities), $h(\hat{p}_{k+1}^-)$ are the corresponding measurement models in (5) and $H_{k+1} = \frac{\partial h(\hat{p}_{k+1}^-)}{\partial \hat{p}_{k+1}^-}$ is the Jacobian matrix of the system measurements.

Given the choice of $\hat{p}_k$, it turns useful to partition the covariance matrix P_k with respect to the vehicle and the map quantities, i.e.

$$P_k = \begin{bmatrix} P_{s,k} & P_{sm,k} \\ P_{sm,k}^T & P_{m,k} \end{bmatrix}, \tag{8}$$

where $P_{s,k} \in \mathbb{R}^{3\times 3}$ is the covariance matrix of the vehicle state s_k, $P_{m,k} \in \mathbb{R}^{2j\times 2j}$ is the covariance matrix of the mapped features uncertainties given the j mapped entities, and $P_{sm,k} \in \mathbb{R}^{3\times 2j}$ is the covariance matrix between the robot and the mapped features. Notice that $P_{s,k}$ and $P_{m,k}$ are the covariances of the marginals of the jointly Gaussian state $\hat{p}_q$. In a delayed mapping algorithm, a new corner feature m_{j+1} it is not added immediately when it is detected but, instead, n consecutive measurements are stored together with the vehicle positions from which they are detected. Hence, two auxiliary vectors $\hat{S}_{n,j,k} = [\hat{s}_k^T, \hat{s}_{k-1}^T, \dots, \hat{s}_{k-n-1}^T]^T$ and $Z_{i,n,k} = [z_{i,k}^T, z_{i,k-1}^T \dots, z_{i,k-n-1}^T]^T$ are stored while the EKF executes. After the n consecutive measures are collected, usually an optimisation technique, such as bundle adjustment [16], is applied to reduce the uncertainty and the new feature is added to the filter state, which is then augmented. The objective of this paper is to make evident the effect of n and to propose a simple method to combine together the delayed measurements.

III. Uncertainty Analysis

To shading alight on the number of measurements n needed before injecting in the EKF the new sensed feature, say m_i, we first define how the measurements in (5), which are collected in the LIDAR frame $\langle L_k \rangle$, are transformed in the fixed reference frame $\langle W \rangle$. Since the origin $O_{l,k}$ undergoes the same motion of the vehicles, the rigid transformation between $\langle L_k \rangle$ and $\langle W \rangle$ will be a function of $\hat{s}_k^T$ as follows (see Figure 1)

$$\overline{m}_{i,q} = \begin{bmatrix} \overline{d}_{i,q}\cos(\overline{\alpha}_{i,q} + \hat{\theta}_q) + \hat{x}_q \\ \overline{d}_{i,q}\sin(\overline{\alpha}_{i,q} + \hat{\theta}_q) + \hat{y}_q \end{bmatrix} = f(b_q). \tag{9}$$

In order to determine the uncertainties involved in this transformation, we first define the vector $b_q = [\hat{s}_q^T, z_{i,q}^T]^T$ containing all the measured and estimated quantities involved in (9) at the generic time qT_s, $q = k-n-1, \dots, k$. By recalling the fact that the EKF is an unbiased estimator and that the uncertainties $\rho_{i,q}$ in (5) are zero-mean, we have immediately that $\mathrm{E}\{b_q\} = [s_q^T, d_{i,q}, \alpha_{i,q}]^T$, i.e the actual values (we use $\mathrm{E}\{\cdot\}$ to denote the expected value). Therefore, the vector $\tilde{b}_q = b_q - \mathrm{E}\{b_q\}$ defines the set of estimation and measurement uncertainties. We can use a first order Taylor approximation of (9) with respect to the mean $\mathrm{E}\{b_q\}$ to determine the uncertainties acting on $\overline{m}_{i,q}$, i.e.

$$\begin{aligned} \overline{m}_{i,q} &\approx f(\mathrm{E}\{b_q\}) + \left.\frac{\partial f(b_q)}{\partial b_q}\right|_{b_q = \mathrm{E}\{b_q\}} (b_q - \mathrm{E}\{b_q\}) = \\ &= m_{i,q} + \begin{bmatrix} M_{i,q}^s & M_{i,q}^h \end{bmatrix} \tilde{b}_q = m_{i,q} + \tilde{m}_{i,q}. \end{aligned} \tag{10}$$

where

$$\begin{aligned} M_{i,q}^s &= \begin{bmatrix} 1 & 0 & -d_{i,q}\sin(\alpha_{i,q} + \theta_q) \\ 0 & 1 & d_{i,q}\cos(\alpha_{i,q} + \theta_q) \end{bmatrix}, \\ M_{i,q}^h &= \begin{bmatrix} \cos(\alpha_{i,q} + \theta_q) & -d_{i,q}\sin(\alpha_{i,q} + \theta_q) \\ \sin(\alpha_{i,q} + \theta_q) & d_{i,q}\cos(\alpha_{i,q} + \theta_q) \end{bmatrix}. \end{aligned} \tag{11}$$

As a consequence of (10), we have that $\mathrm{E}\{\overline{m}_{i,q}\} = m_{i,q}$. Moreover, to compute the covariance matrix of $\tilde{m}_{i,q}$, we first compute $B_q = \mathrm{E}\left\{\tilde{b}_q \tilde{b}_q^T\right\} = \mathrm{diag}(P_{s,q}, R)$, where $P_{s,q}$ is defined in (8), while R is the covariance matrix of the measurement uncertainties in (5). Notice that B_q is block diagonal since the i-th new feature has not yet been added to the EKF. Therefore

$$F_{i,q} = \mathrm{E}\left\{\tilde{m}_{i,q}\tilde{m}_{i,q}^T\right\} = \begin{bmatrix} M_{i,q}^s & M_{i,q}^h \end{bmatrix} B_q \begin{bmatrix} {M_{i,q}^s}^T \\ {M_{i,q}^h}^T \end{bmatrix}. \tag{12}$$

It is worthwhile to note that $\tilde{m}_{i,q}$ and $\tilde{m}_{i,q+a}$, $\forall a \in \mathbb{Z}$, are correlated due to the presence of the state estimates $\hat{s}_q$ and $\hat{s}_{q+a}$, which are correlated by the recursive nature of the EKF and whose covariance matrix is $P_{s,q,q+a}$. In particular,

$$\begin{aligned} \mathrm{E}\left\{\tilde{m}_{i,q}\tilde{m}_{i,q+a}^T\right\} &= \begin{bmatrix} M_{i,q}^s & M_{i,q}^h \end{bmatrix} \begin{bmatrix} P_{s,q,q+a} & 0 \\ 0 & 0 \end{bmatrix} \begin{bmatrix} {M_{i,q+a}^s}^T \\ {M_{i,q+a}^h}^T \end{bmatrix} = \\ &= M_{i,q}^s P_{s,q,q+a} {M_{i,q+a}^s}^T = F_{i,q,q+a}. \end{aligned} \tag{13}$$

Ideally, the i-th new feature estimate $\hat{m}_i$ to be injected in the EKF state after n steps can be obtained by a Weighted Least Squares (WLS) solution

$$\hat{m}_i = (\mathbf{I}_{n-1}^T F_i^{-1} \mathbf{I}_{n-1})^{-1} \mathbf{I}_{n-1}^T F_i^{-1} \begin{bmatrix} \overline{m}_{i,k}^T & \dots & \overline{m}_{i,k-n-1}^T \end{bmatrix}^T,$$

where the indirect measurements $\overline{m}_{i,q}$ are given by (9), $\mathbf{I}_{n-1}$ is a matrix having $n-1$ identity matrices of dimension 2 stacked one after the other one and F_i has on the diagonal the matrices $F_{i,q}$ in (12), $q = k-n-1, \dots, k$, and off-diagonal the matrices $F_{i,q,q+a}$ in (13), $a = -n, \dots, -1$. Moreover the uncertainties on $\hat{m}_i$ are zero-mean (due to (5)) and with covariance matrix

$$\mathrm{E}\left\{\tilde{m}_i \tilde{m}_i^T\right\} = (\mathbf{I}_{n-1}^T F_i^{-1} \mathbf{I}_{n-1})^{-1}, \tag{14}$$

which is lower than the single indirect measurements uncertainties $F_{i,q}$, $q = k-n-1, \dots, k$, in (12) due to the property of the EKF and of the WLS. However, in order to numerically compute F_i the actual values of the state s_q and of the measurements $h(s_q, m_i)$ in (5) are needed, which are of course unknown. One shortcut that appears feasible and effective is to actually consider F_i as an identity matrix, which amounts to compute

$$\hat{m}_i = \frac{1}{n} \sum_{l=0}^{n-1} \overline{m}_{i,k-l}. \tag{15}$$

Adopting the sample mean simplifies the computation and still exhibits a filtering behaviour, nonetheless neglecting the covariances and assuming all the measurements are equally uncertain leads to an uncertainty for this estimator that have a covariance matrix worse than (14). To account for this effect, we precautionary assume the uncertainty equal to the measurements uncertainty, hence $\mathrm{E}\left\{\tilde{m}_i \tilde{m}_i^T\right\} = \hat{F}_{i,k}$ in (12) evaluated using the EKF estimates $\hat{s}_k$ and the measurements $z_{i,k}$ available at time kT_s.

Once the estimates are available, the i-th feature is injected in the EKF at time kT_s with the following updates:

$$\begin{aligned} \hat{p}_k = [\hat{s}_k^T, \hat{\mathcal{M}}_{j,k}^T]^T \to [\hat{s}_k^T, \hat{\mathcal{M}}_{j,k}^T, \hat{m}_{i,k}^T]^T = [\hat{s}_k^T, \hat{\mathcal{M}}_{j+1,k}^T]^T, \\ P_k \to \begin{bmatrix} P_k & P_{sm,i,k} \\ P_{sm,i,k}^T & \hat{F}_{i,k} \end{bmatrix}, \end{aligned} \tag{16}$$

where

$$P_{sm,i,k} = \mathrm{E}\left\{\tilde{p}_k \tilde{b}_k^T\right\} \begin{bmatrix} (\hat{M}_{i,k}^s)^T \\ (\hat{M}_{i,k}^h)^T \end{bmatrix} = \begin{bmatrix} P_{s,k} \\ P_{sm,k}^T \end{bmatrix} (\hat{M}_{i,k}^s)^T, \tag{17}$$

where $\hat{M}_{i,k}^s$ is evaluated using the EKF estimates $\hat{s}_k$ and the measurements $z_{i,k}$ available at time kT_s. Since the EKF uses the mapped features to bound the uncertainties on $\hat{s}_k$, the number of steps n used to lower down the uncertainties on the new features will be a function of the measurement uncertainties acting on the encoders ε_k and on the LIDAR $\rho_{i,k}$, as shown in Section IV.

A. Range-only SLAM

We will here derive the solution when only the ranging measurements $\overline{d}_{i,k}$ in (5) are available. In this case, the analysis follows the trilateration (or multilateration) idea followed in localisation problems [18].

1) One delayed step: $n = 1$: We first notice that considering just one ranging measurement, the feature can be located in a circumference with radius $\overline{d}_{i,k}$ and centred in the robot position, which is reflected by rewriting $\overline{d}_{i,k}$ in (5) in terms of its square and then solve with respect to $\overline{x}_i$, i.e.

$$\overline{x}_i = \hat{x}_k - \sqrt{\overline{d}_{i,k}^2 - (\hat{y}_k - \overline{y}_i)^2} = f(b_k), \tag{18}$$

where $\mathrm{E}\{b_k\} = [s_k^T, d_{i,k}, \overline{y}_i]^T$. We first notice that $\overline{y}_i$ is limited by the constraint on the positiveness of the argument of the square root in (18), which yields immediately that $\overline{y}_i \sim \mathcal{U}(\hat{y}_k - \overline{d}_{i,k}, \hat{y}_k + \overline{d}_{i,k})$, i.e. a uniformly distributed random variable with mean value $\mathrm{E}\{\overline{y}_i\} = \hat{y}_k$ and variance $\sigma_{\overline{y}_i}^2 = \mathrm{E}\{(\overline{y}_i - \hat{y}_k)\} = \frac{d_{i,k}^2}{3}$. It then follows that, following the same steps in (10) the first order linearised relation in (18) boils down to

$$\begin{aligned} \overline{x}_i &\approx x_i + \begin{bmatrix} 1 & \frac{-2\tilde{y}_k}{\sqrt{d_{i,k}^2 - \tilde{y}_k^2}} & 0 & \frac{-2d_{i,k}}{\sqrt{d_{i,k}^2 - \tilde{y}_k^2}} & \frac{2\tilde{y}_k}{\sqrt{d_{i,k}^2 - \tilde{y}_k^2}} \end{bmatrix} \tilde{b}_k = \\ &= x_i + M_{i,k} \tilde{b}_k, \end{aligned}$$

and $\mathrm{E}\left\{\tilde{b}_k \tilde{b}_k^T\right\} = \mathrm{diag}(P_{s,k}, \sigma_d^2, \frac{d_{i,k}^2}{3})$. As a consequence, the variance of $\overline{x}_i$ will be $\sigma_{\overline{x}_i}^2 = M_{i,k} \mathrm{E}\left\{\tilde{b}_k \tilde{b}_k^T\right\} M_{i,k}^T$. Therefore, the state of the EKF will be updated with (16), where

$$\hat{F}_{i,k} = \begin{bmatrix} \hat{\sigma}_{\overline{x}_i}^2 & \frac{2\tilde{y}_k}{\sqrt{\overline{d}_{i,k}^2 - \tilde{y}_k^2}} \hat{\sigma}_{\overline{y}_i}^2 \\ \frac{2\tilde{y}_k}{\sqrt{\overline{d}_{i,k}^2 - \tilde{y}_k^2}} \hat{\sigma}_{\overline{y}_i}^2 & \hat{\sigma}_{\overline{y}_i}^2 \end{bmatrix},$$

where $\hat{\sigma}_{\overline{x}_i}^2$ and $\hat{\sigma}_{\overline{y}_i}^2$ are computed using $\hat{s}_k$, $\overline{d}_{i,k}$, as in the previous case, plus a randomly generated value for $\tilde{y}_k$ generated according to $P_{s,k}$. Finally, the value injected in the EKF will be $\hat{m}_{i,k}$ whose $\overline{x}_{i,k}$ is given by (18) and $\overline{y}_{i,k}$ is a randomly generated number from $\mathcal{U}(\hat{y}_k - \overline{d}_{i,k}, \hat{y}_k + \overline{d}_{i,k})$, while the covariance matrix is updated according to (16) and (17).

2) Two delayed steps: $n = 2$: Considering two consecutive ranging measurements taken from two different locations at time kT_s and $(k-1)T_s$ (i.e. $v_{k-1} T_s \neq 0$ in (4)), the problem may be intractable. Indeed, using the fact that two ranging measurements from two distinct locations corresponds to the intersection of two circles, we end-up with two different hypothesis for $\hat{m}_i$, which actually violates the unimodal assumption of the EKF. A possible way to circumvent the problem is to take two consecutive measures as for $n = 1$ and then average them. The rest of the analysis is then similar to the previous case.

3) More than two delayed steps: $n \geq 3$: In this case, we can apply trilateration ($n = 3$) or multilateration ($n > 3$) to have an estimate of $\hat{m}_i$ before it is injected in the EKF. Indeed,

by writing the difference of the squares of the distances in (5) we immediately have

$$\begin{bmatrix} \overline{d}^2_{i,k} - \overline{d}^2_{i,k-1} - \hat{x}^2_k + \hat{x}^2_{k-1} - \hat{y}^2_k + \hat{y}^2_{k-1} \\ \overline{d}^2_{i,k} - \overline{d}^2_{i,k-2} - \hat{x}^2_k + \hat{x}^2_{k-2} - \hat{y}^2_k + \hat{y}^2_{k-2} \\ \vdots \\ \overline{d}^2_{i,k} - \overline{d}^2_{i,k-n-1} - \hat{x}^2_k + \hat{x}^2_{k-n-1} - \hat{y}^2_k + \hat{y}^2_{k-n-1} \end{bmatrix} =$$

$$= -2 \begin{bmatrix} \hat{x}_k - \hat{x}_{k-1} & \hat{y}_k - \hat{y}_{k-1} \\ \hat{x}_k - \hat{x}_{k-2} & \hat{y}_k - \hat{y}_{k-2} \\ \vdots & \\ \hat{x}_k - \hat{x}_{k-n-1} & \hat{y}_k - \hat{y}_{k-n-1} \end{bmatrix} \overline{m}_i \Rightarrow D_{i,k,n} = C_{k,n} \overline{m}_i.$$

Therefore, we have immediately a Least Squares (LS) solution

$$\overline{m}_i = (C^T_{k,n} C_{k,n})^{-1} C^T_{k,n} D_{i,k,n}, \tag{19}$$

which is the closed form solution for a number of steps $n \geq 3$ and plays the role of (9). In the interest of space, we are omitting the explicit form of the solution that can be obtained following the same steps depicted for the range and bearing case. However, we can notice that the LS solution is feasible if and only if $\omega_q \neq 0$, $q = k-n-1, \ldots, k-1$, i.e. the landmark is observed from positions with different orientations θ_k [19], otherwise the rows of $C_{k,n}$ are linearly dependent (in such a case, the solution with one-delayed step is still feasible and the only feasible). Moreover, even if the rows are linearly independent, due to encoder uncertainties ε_k (4), the matrix $C^T_{k,n} C_{k,n}$ in (19) may be close to singularity and, hence, generating high estimation uncertainties: in this case, we expect that a higher number of delayed steps n may be beneficial to increase the accuracy.

IV. Simulation Results

Fifty different simulations have been carried out for each test case to show the effect of the delayed mapping steps n on the vehicle and feature uncertainties. In the presented results we have considered a sampling time $T_s = 100$ ms. For the ego-motion estimation, we have considered a typical robotic vehicle having the wheels radius $r = 5$ cm, the inter-axle length $l = 30$ cm and the uncertainties on the wheel encoder readings generating ε_k in (4) of $\sigma_r = \sigma_l = 0.002$ rad, as reported in [20]. For the LIDAR characterisation, we have considered a maximum range reading of 15 m and the angle swept by the sensor to be limited to $\pm\pi/2$ rad, with the zero angle oriented with the robot forward direction (i.e. the axis $X_{l,k}$ in Figure 1). Moreover, the sensor reading uncertainties in (5) are respectively $\sigma_d = 2$ cm and $\sigma_\alpha = 0.7$ mrad, as the worst case situation reported in [21] for commercial LIDARs.

In the simulations, the robot is supposed to start in position $s_0 = [3\text{ m}, 3\text{ m}, 0\text{ rad}]^T$ (which is known as for any SLAM problem) and moving in synthetic indoor environments (an example is shown in Figure 1 with the followed path and the mapped features). The estimation uncertainty on the robot pose $\tilde{s}_k$ and on the landmark positions $\tilde{m}_i$ along a sample trajectory are easily visible in Figure 2 for $n = 1$, i.e. no delayed mapping and standard SLAM approach. The distance

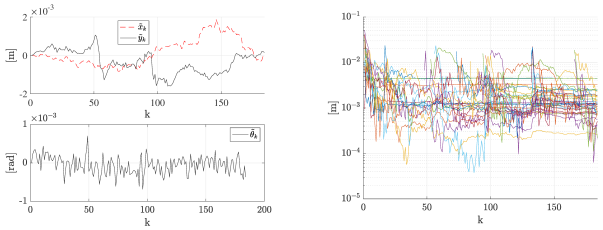

(a) (b)

Fig. 2. (a) Robot pose estimation error and (b) mapped features estimation errors (i.e. distance error of each landmark $\sqrt{\tilde{m}_i^T \tilde{m}_i}$, $\forall i$) for $n = 1$.

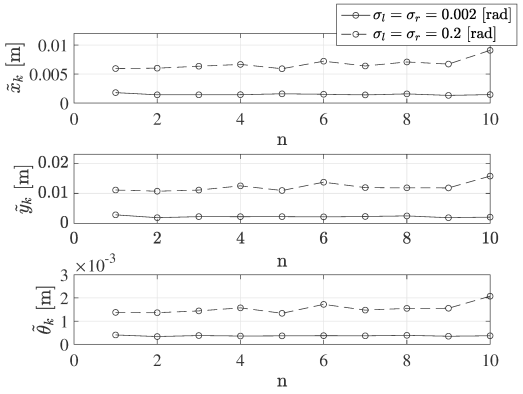

Fig. 3. RMSE for the robot pose error $\tilde{s}_k$ versus the number of steps of the delayed mapping n in nominal conditions (solid line) and with an increase of 100 times of the encoder uncertainties (dashed line).

error of each landmark, i.e. $\sqrt{\tilde{m}_i^T \tilde{m}_i}$, $\forall i$, is reported. For a quantitative analysis of the effects of the delayed SLAM when the simple proposed average approach in (15) is considered, we report in Figure 3 the Root Mean Squared Error (RMSE) plot of the vehicle pose as a function of the number of steps n adopted. It turns out that averaging with at least two measurements (i.e. $n = 2$) contributes in the reduction of the uncertainty (solid line in Figure 3). Of course, if the uncertainties on the ego-motion increases (dashed line), averaging has a detrimental effect since in (15) the robot state estimates $\hat{s}_k$ have an increasing non-negligible uncertainty. To further evaluate the solution and provide a clear clue about the role of the measurement uncertainties, we report in Figure 4 the RMSE of the vehicle pose when the range uncertainties is ten times higher (i.e. $\sigma_d = 20$ cm) or when the angle uncertainty is ten (i.e. $\sigma_\alpha = 7$ mrad, solid line) to one hundred times (i.e. $\sigma_\alpha = 70$ mrad, dashed line) higher than the nominal values. From these results, it is evident that the ranging error has a higher effect than the angle error on the state estimation uncertainties $\tilde{s}_k$, while using a delayed approach in this case worsen the performances, i.e. the chosen averaging approach is worse that then linearised EKF. Instead, for the angle error, the delayed mapping plays a beneficial effect (Figure 4-b) that becomes more evident as the uncertainty σ_α increases.

For what concern the range-only delayed mapping SLAM, we report in Figure 5 the RMSE results for both the robot

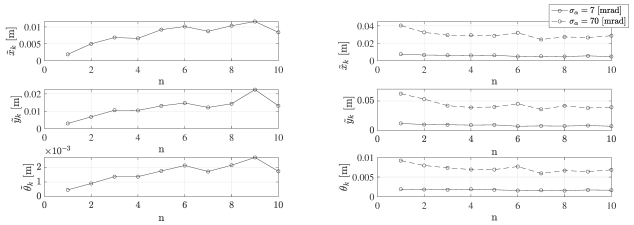

(a) (b)

Fig. 4. (a) RMSE for higher range error (i.e. $\sigma_d = 20$ cm). (b) RMSE for higher angular error (i.e. $\sigma_\alpha = 7$ mrad)). Both graphs are expressed as a function of the number of steps n in the delayed mapping.

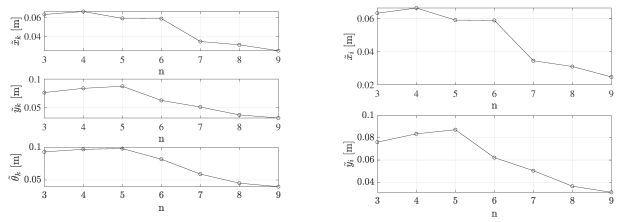

(a) (b)

Fig. 5. (a) Localisation RMSE and mapping RMSE (b) for the range-only case. Both graphs are expressed as a function of the number of steps n in the delayed mapping SLAM.

localisation and the landmark estimates as a function of $n \geq 3$, i.e. when trilateration becomes feasible. As can be seen from the picture, it is evident how a larger n benefits both the robot localisation and the feature mapping. This is clearly dictated by the role of the uncertainties in (19) that can make the matrix $C_{k,n}^T C_{k,n}$ close to singularity when n is small.

V. Conclusions

An uncertainty driven analysis of the delayed SLAM for a robot moving in an indoor environments and equipped with a LIDAR sensor is provided in this paper. The theoretical analysis, provided in terms of range and bearing and range-only measurements, is tested in simulations using a synthetic indoor environment and exposing the effects of the delayed window length n on the localisation and mapping uncertainties. Extensions of this work will be provided in the next future by including the analysis for bearing-only measurements, i.e. considering only the angle measurements in (5) and by providing an analysis about the role of the uncertainties ε_k in (4) in the matrix $C_{k,n}^T C_{k,n}$ reported in (19) against numerical errors. Moreover, we will explore the applicability of the multiple-model EKF with likelihood weighting to deal with multimodality of the estimates and we will provide an actual implementation on a robotic system.

References

[1] H. Durrant-Whyte and T. Bailey, "Simultaneous localization and mapping: part I," *IEEE Robotics Automation Magazine*, vol. 13, no. 2, pp. 99–110, 2006.

[2] T. Bailey and H. Durrant-Whyte, "Simultaneous localization and mapping (SLAM): part II," *IEEE Robotics Automation Magazine*, vol. 13, no. 3, pp. 108–117, 2006.

[3] F. A. Belo, P. Salaris, D. Fontanelli, and A. Bicchi, "A Complete Observability Analysis of the Planar Bearing Localization and Mapping for Visual Servoing with Known Camera Velocities," *Intl. Journal of Advanced Robotic Systems*, vol. 10, no. 197, pp. 1–9, 2013.

[4] R. Giubilato, S. Chiodini, M. Pertile, and S. Debei, "Minivo: Minimalistic range enhanced monocular system for scale correct pose estimation," *IEEE Sensors Journal*, vol. 20, no. 20, pp. 11 874–11 886, 2020.

[5] R. Mur-Artal and J. D. Tardós, "Orb-slam2: An open-source slam system for monocular, stereo, and rgb-d cameras," *IEEE Transactions on Robotics*, vol. 33, no. 5, pp. 1255–1262, 2017.

[6] M. Montemerlo, S. Thrun, D. Koller, B. Wegbreit *et al.*, "Fastslam 2.0: An improved particle filtering algorithm for simultaneous localization and mapping that provably converges," in *IJCAI*, 2003, pp. 1151–1156.

[7] J. Deschaud, "Imls-slam: Scan-to-model matching based on 3d data," in *2018 IEEE International Conference on Robotics and Automation (ICRA)*, 2018, pp. 2480–2485.

[8] R. Milijaš, J. Oršulić, and S. Bogdan, "When measurements fail: using an interactive slam solution to fight bad odometry," in *2020 IEEE International Instrumentation and Measurement Technology Conference (I2MTC)*, 2020, pp. 1–6.

[9] R. Munguia and A. Grau, "Closing loops with a virtual sensor based on monocular slam," *IEEE Transactions on Instrumentation and Measurement*, vol. 58, no. 8, pp. 2377–2384, 2009.

[10] J. Jung, S. Lee, and H. Myung, "Indoor mobile robot localization and mapping based on ambient magnetic fields and aiding radio sources," *IEEE Transactions on Instrumentation and Measurement*, vol. 64, no. 7, pp. 1922–1934, 2015.

[11] R. Giubilato, S. Chiodini, M. Pertile, and S. Debei, "An evaluation of ros-compatible stereo visual slam methods on a nvidia jetson tx2," *Measurement*, vol. 140, pp. 161 – 170, 2019.

[12] B. Park and H. Myung, "Underground localization using dual magnetic field sequence measurement and pose graph SLAM for directional drilling," *Measurement Science and Technology*, vol. 25, no. 12, p. 125101, oct 2014.

[13] M. D. Pereira, O. Postolache, and P. S. Girao, "Using neural network techniques in environmental sensing and measurement systems to compensate for the effects of influence quantities," *IEEE Instrumentation Measurement Magazine*, vol. 17, no. 6, pp. 26–56, 2014.

[14] D. DeTone, T. Malisiewicz, and A. Rabinovich, "Superpoint: Self-supervised interest point detection and description," in *Proceedings of the IEEE Conference on Computer Vision and Pattern Recognition (CVPR) Workshops*, June 2018.

[15] T. Zhang, K. Wu, J. Song, S. Huang, and G. Dissanayake, "Convergence and consistency analysis for a 3-d invariant-ekf slam," *IEEE Robotics and Automation Letters*, vol. 2, no. 2, pp. 733–740, 2017.

[16] M. Deans and M. Hebert, "Experimental comparison of techniques for localization and mapping using a bearing-only sensor," in *Experimental Robotics VII*. Springer, 2001, pp. 395–404.

[17] Y.-T. Wang, C.-C. Peng, A. A. Ravankar, and A. Ravankar, "A single lidar-based feature fusion indoor localization algorithm," *Sensors*, vol. 18, no. 4, p. 1294, 2018.

[18] L. Palopoli, D. Macii, and D. Fontanelli, "A Positioning Filter based on Uncertainty and Observability Analyses for Nonholonomic Robots," in *Proc. IEEE Int. Instrumentation and Measurement Technology Conference (I2MTC)*. Dubrovnik, Croatia: IEEE, May 2020, pp. 1–6.

[19] L. Palopoli and D. Fontanelli, "Global Observability Analysis of a Nonholonomic Robot using Range Sensors," in *European Control Conference (ECC)*. Saint Petersburg, Russia: IFAC, May 2020, pp. 1300–1305.

[20] P. Nazemzadeh, D. Fontanelli, D. Macii, and L. Palopoli, "Indoor Localization of Mobile Robots through QR Code Detection and Dead Reckoning Data Fusion," *IEEE/ASME Transactions on Mechatronics*, vol. 22, no. 6, pp. 2588–2599, Dec. 2017.

[21] C. Glennie, "Rigorous 3d error analysis of kinematic scanning lidar systems," *Journal of Applied Geodesy*, vol. 1, no. 3, p. 147, 2007.